THE JOURNAL OF PHYSICAL CHEMISTRY LETTERS
A JOURNAL OF THE AMERICAN CHEMICAL SOCIETY

pubs.acs.org/JPCL

Letter

Ultrasensitive Label-Free Detection of Protein–Membrane Interaction Exemplified by Toxin-Liposome Insertion

T. Schönfeldová, H. I. Okur, V. Vezočnik, I. Iacovache, C. Cao, M. Dal Peraro, P. Maček, B. Zuber, and S. Roke*

Cite This: J. Phys. Chem. Lett. 2022, 13, 3197–3201

Read Online

ACCESS | Metrics & More | Article Recommendations | Supporting Information

ABSTRACT: Measuring the high-affinity binding of proteins to liposome membranes remains a challenge. Here, we show an ultrasensitive and direct detection of protein binding to liposome membranes using high throughput second harmonic scattering (SHS). Perfringolysin O (PFO), a pore-forming toxin, with a highly membrane selective insertion into cholesterol-rich membranes is used. PFO inserts only into liposomes with a cholesterol concentration >30%. Twenty mole-percent cholesterol results in neither SHS-signal deviation nor pore formation as seen by cryo-electron microscopy of PFO and liposomes. PFO inserts into cholesterol-rich membranes of large unilamellar vesicles in an aqueous solution with K_d = $(1.5 \pm 0.2) \times 10^{-12}$ M. Our results demonstrate a promising approach to probe protein–membrane interactions below sub-picomolar concentrations in a label-free and noninvasive manner on 3D systems. More importantly, the volume of protein sample is ultrasmall (<10 μL). These findings enable the detection of low-abundance proteins and their interaction with membranes.

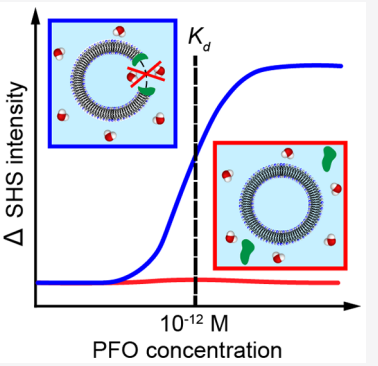

Lipid membranes serve as a hub for vital biochemical reactions and play an important role in chemical signaling.[1] Membrane–protein interactions are characterized by sparse, high-affinity, and highly specific binding interactions that lead to specific responses.[2] Membrane channels and pores are examples of the result of such interactions, keeping specific chemicals in- or outside of the cell or organelle to maintain the function of the organism. Pores are also used by bacteria for the opposite effect: to invade cells by effectively punching a hole in the membrane.[3] These pore-forming toxins (PFTs) have highly specific membrane interactions, often requiring specific receptors, certain membrane composition, and an aqueous environment. One example is perfringolysin O (PFO, depicted in Figure 1A), which is a representative of the cholesterol-dependent cytolysin family. PFO is a soluble elongated 4-domain protein that is rich in β sheets and is produced by the pathogenic *Clostridium perfringens*.[4] PFO has been demonstrated to selectively interact with cholesterol-rich membranes[5] where it self-assembles into a barrel-like 38-nm-wide structure of up to 50 monomers[6] (see Figure 1A). The monomeric structure of PFO was obtained by X-ray crystallography,[5] while its oligomer structure has been characterized by combining information about the monomeric form, cryo-electron microscopy (cryo-EM) data of pneumolysin,[7] and molecular dynamics (MD) simulations.[8] Figure 1B shows cryo-EM images of 120-nm-diameter-large unilamellar vesicles (LUVs) with membranes composed of sphingomyelin (SM) and cholesterol (Chol) at 50:50 mol % (1B i, iii, iv) and at 80:20 mol % (Figure 1B, ii). The PFO clearly displays strong interactions with the membrane in images i, iii, and iv, while no interaction is observed in ii. This is consistent with previous studies[7,9] that show fully inserted pores in the membranes that have 50:50 mol % of SM:Chol.

To understand the protein–membrane interaction beyond the crystallographic level, currently used methods are quartz crystal microbalance (QCM),[10−12] flotation assays,[13] surface plasmon resonance (SPR),[14−18] calorimetric methods,[19] and different fluorescence approaches.[20−22] Although these methods provide information about binding kinetics, they require a large amount of sample and the sensitivity is limited; namely, it does not allow the detection of low-abundance proteins whose concentration is below micromolarity. Besides the limited sensitivity, fluorimetry requires the labeling/binding of a fluorophore, which may alter the chemical and/or structural properties of the target membrane proteins, thereby perturbing the native binding affinity with the membrane. Likewise, QCM and SPR are indirect methods that require a specific substrate, which restricts the application mostly to planar-supported model membranes, and calorimetry lacks specificity to a binding event. Resonant reflection second harmonic generation (SHG) has recently been successfully employed and suggested as an alternative to immunoassays[23,24] since the SH

Received: December 9, 2021
Accepted: March 29, 2022

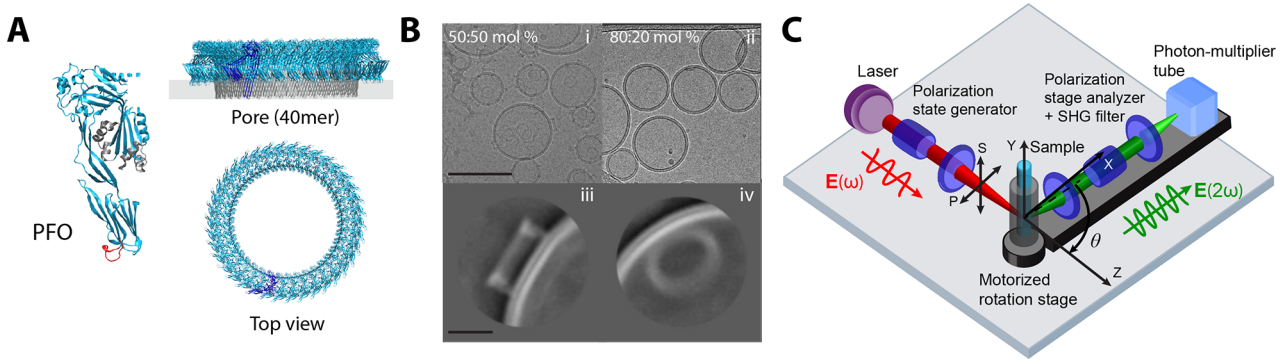

Figure 1. The PFO structure, the PFO-membrane interaction, and the high-throughput second harmonic scatteringsetup. (A) The structure of the PFO:PFO monomer with the undecapeptide, located on domain 4, that binds to cholesterol shown in red, PFO membrane insertion where one pore consists of 40 protomers, and a top view of such a pore. This figure is adapted from ref 3. (B) Cryo-EM images of SM:Chol 50:50 mol % (i) and 80:20 mol % (ii) LUVs measured with the same concentration of PFO in the solution ($c = 9 \times 10^{-6}$ M). 2D classifications of cryo-EM images of oligomerization on the SM:Chol 50:50 mol % membrane from the side (iii) and top (iv). The scale bar corresponds to 200 nm for i and ii, and to 20 nm for iii and iv, respectively. (C) Illustration of the SHS setup. All measurements were recorded with all beams polarized in the horizontal plane leading to a PPP polarization combination. For the single angle experiments, the scattering angle θ was set to 45° corresponding to the angle with maximum scattering intensity.

photons emerge directly from an interface and thus facilitate direct detection of interfacial events. In these experiments, the SH photons were generated via a total internal reflection scheme from a UV resonant interaction (266 nm). Further improvements should allow for nonresonant detection, with high sensitivity, from any type of realistic membrane interface, such as that of a liposome.

Here, we show a method to detect protein liposome interaction using membrane interfacial water as a contrast agent and demonstrate sensitivity in the femtomolar range, using small volumes of protein solution. High throughput second harmonic scattering[25] (Figure 1C) has been shown to be a label-free method using the detection of interfacial water on buried interfaces in aqueous solution, e.g., liposomes[26,27] and oil droplets.[28] In a nonresonant SHS experiment, a pulsed femtosecond near-infrared laser beam interacts with the liposome solution. SH photons are emitted from all noncentrosymmetric molecules that are noncentrosymmetrically distributed. Since interfacial water is noncentrosymmetrically distributed while bulk liquid is not, SHS has an exquisite interfacial sensitivity. The interfacial water outnumbers lipids with a ratio of >1:100, and due to the nonresonant nature of the process both constituents respond with electromagnetic fields that have equal magnitudes. Because the SH intensity scales quadratically with the emitted electromagnetic field, SHS generally reports on membrane hydration, detecting the net orientational distribution of water molecules along the surface normal. The response of the water has been successfully used to quantify physio-chemical interfacial properties, such as the electrostatic potential (Φ_0) and the degree of water ordering (quantified by the second-order susceptibility, $\chi^{(2)}_{s,2}$).[29,30] A recent study has also shown that changes in the membrane water can help understand the interaction of α-synuclein and the aqueous environment of liposomes.[31] Building onto these findings, we use high-throughput SHS to investigate the binding of a transmembrane protein, taking PFO as an example (Figure 2A as an illustration). We demonstrate sensitivity in the femtomolar range and determine a PFO-liposome binding rate of $(1.5 \pm 0.2) \times 10^{-12}$ M.

To test the suitability of SHS measurements for ultrasensitive detection of transmembrane protein−membrane interactions, we employ PFO protein−lipid membrane interaction events, comparing the two membrane systems of Figure 1B, using a 50:50 mol % ratio of SM:Chol and an 80:20 mol % ratio of SM:Chol, whereby protein binding/insertion occurs only in the first case. Figure 2 shows ζ-potential values (Figure 2B) and SHS scattering patterns (Figure 2C) obtained for dispersions of LUVs with a 120 nm radius and with a 50:50 mol % ratio of SM:Chol. Adding 1 pM and 1 nM of PFO to the solution does not change the ζ-potential but does change the intensity of the SHS patterns. The SH intensity arises from coherent light scattering by oriented interfacial water. This water is either oriented by chemical interfacial interactions (such as hydrogen bonding, dipole−dipole, or van der Waals interactions) or by interfacial electrostatic effects. Within the nonlinear light scattering theory that is used to describe this type of data, both interactions are captured by distinct physical parameters, namely the interfacial second-order susceptibility ($\chi^{(2)}_{s,2}$) and the surface potential (Φ_0). Since the membrane interaction event of PFO is interpreted to result in the appearance of a hole, the effect on the interfacial structure of water is to reduce the number of interfacially oriented water molecules due to the lack of membrane induced anisotropy, as the interfacial area is reduced (see Figure 2A for an illustration). Therefore, the change in SHS response arises from a modification of the surface susceptibility rather than the surface potential. This is confirmed by the ζ-potential data, which shows no PFO-induced changes. Further verification is obtained from the shape of the scattering patterns for different PFO concentrations: since the $\chi^{(2)}_{s,2}$ and Φ_0 terms are weighted by different scattering angle-dependent form factor functions, the SHS patterns do not change shape as the PFO concentration is increased. It means that the intensity changes must either come from changes in $\chi^{(2)}_{s,2}$ or from changes in Φ_0 but not from simultaneous changes.

The coherent normalized SHS intensity patterns ($S(2\omega, \theta)$) of Figure 2C are thus the sum of the scattering patterns of individual bare LUVs ($s_L(2\omega, \theta)$) and LUVs that have a PFO protein ($s_{LP}(2\omega, \theta)$) inserted. With N_0 being the original

https://doi.org/10.1021/acs.jpclett.1c04011
J. Phys. Chem. Lett. 2022, 13, 3197−3201

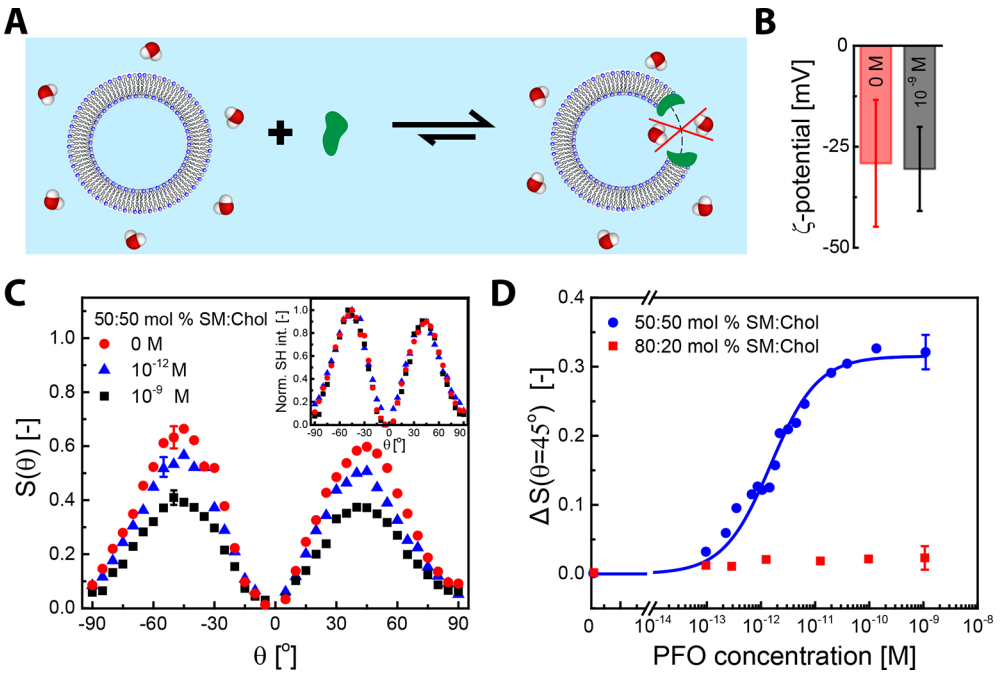

Figure 2. PFO-vesicle binding. (A) Illustration of PFO insertion into 50:50 mol % ratio of SM:Chol LUVs surrounded by water. The pore insertion is expected to modulate the SHS intensity by removing a significant part of the membrane. Without this membrane, the number of interfacially oriented water molecules is reduced due to a lack of membrane induced anisotropy (blue color represents the aqueous medium, and the water molecules that contribute to the SHS signal are emphasized; for simplicity the molecularly complicated interaction is here shown as the formation of a hole). (B) Measured ζ-potential of the 50:50 mol % SM:Chol LUVs with 0 M and 10^{-9} M of PFO. (C) SHS patterns of 50:50 mol % SM:Chol LUVs with 0 M (red circles), 10^{-12} M (blue triangles), and 10^{-9} M (black squares) of PFO recorded using the PPP polarization combination. The inset shows normalized SHS patterns. The error bars were determined as a standard deviation from 20 measurements. (D) SH intensity difference (ΔS) at the angle with the maximum intensity (θ_{max} = 45°) vs PFO concentration in logarithmic scale for two different LUV membrane compositions, SM:Chol 50:50 mol % (blue circles) and 80:20 mol % (red squares). ΔS is a difference between the coherent signal from the vesicles with a given concentration of PFO and the vesicles without PFO (with the highest number of interfacially oriented water molecules). The error bars were determined as a standard deviation from 100 measurements. The data of SM:Chol 50:50% are fitted using eq 5, giving the dissociation constant $K_d = (1.5 \pm 0.2) \times 10^{-12}$ M.

number of liposomes and N the number of liposomes with a bound protein, we obtain for the total intensity:

$$S(2\omega, \theta) = (N_0 - N)s_L(2\omega, \theta) + Ns_{LP}(2\omega, \theta) = N(s_{LP}(2\omega, \theta) - s_L(2\omega, \theta)) + N_0 s_L(2\omega, \theta) \quad (1)$$

The relation between the coherent SH intensity ($I(2\omega, \theta)$) and the plotted response ($S(2\omega, \theta)$) is given by eq S1 in the SI. Having confirmed that the SHS response arises purely from the degree of water ordering at the interface, we performed measurements at the scattering angle of maximum intensity (θ_{max}, Figure 2C). Figure 2D displays the difference in SH response, $\Delta S = |S(2\omega, \theta) - S_L(2\omega, \theta)|$, where $S_L(2\omega, \theta)$ is the coherent water normalized SHS intensity from liposomes without PFO, as a function of the PFO concentration in the solution. We employ two types of LUVs, composed of 80:20 mol % (red squares) and 50:50 mol % (blue circles) SM:Chol, respectively. The first LUVs with lower Chol contents show no apparent change in the SHS intensity, while those with 50 mol % Chol exert a gradual increase at ~100 fM and a rapid rise around ~1 pM of PFO. The SH intensity difference levels off at 10 nM, which represents the saturation of the system meaning that no more proteins can bind to the liposomes. This protein-induced change in the intensity is reminiscent of a Langmuir isotherm. We describe this interaction as an equilibrium, to retrieve N (the number of liposomes assumed to have a (pre)pore (Figure 2A)) to obtain an expression for the measured SHS intensity difference. The PFO (P) binding to liposomes (L) can simplistically be described by

$$L + P \rightleftharpoons_{k_{-1}}^{k_1} LP \quad (2)$$

This follows a kinetic equation relating the rate of insertion (k_1) to the change in the number of liposomes with a PFO (N):

$$\frac{dN}{dt} = k_1(N_0 - N) - k_{-1}N \quad (3)$$

At equilibrium conditions ($dN/dt = 0$), we then have

$$N = \frac{N_0}{K_d + 1} \quad (4)$$

where $K_d = k_{-1}/k_1$ is the equilibrium PFO binding/insertion constant. Connecting this to eq 1, the measured difference in the coherent SH intensity of Figure 2D then becomes

$$\Delta S = |S(2\omega, \theta) - S_L(2\omega, \theta)| = |N(s_{LP} - s_L)| = |N\Delta s| = \left|\frac{N_0 \Delta s}{K_d + 1}\right| \quad (5)$$

Applying this expression to the data in Figure 2D, we obtain a pore insertion constant of $K_d = (1.5 \pm 0.2) \times 10^{-12}$ M.

Using the high throughput angle-resolved SHS technique, we thus demonstrate ultrasensitive detection of protein binding to liposomes. This is of special interest since standard methods

https://doi.org/10.1021/acs.jpclett.1c04011
J. Phys. Chem. Lett. 2022, 13, 3197−3201

require working on a supported lipid bilayer or surface-attached vesicles. QCMD or other mass-based binding assays lose sensitivity at weights less than nanograms of protein. SPR-based technologies require kinetic data for recording and modeling, which limits their sensitivity in the micromolar range. In addition, SHS as presented here does not require any planar substrate and can utilize free-floating liposomes in an aqueous environment. Moreover, the obtained SHS data are quantifiable and could be extended in the following ways: Obtained values for the binding constant, the second-order surface susceptibility of water, and the electrostatic surface potential[23] could be connected with MD simulations as is currently done for X-ray crystallography and cryo-electron microscopy. In fact, if MD-predicted molecular conformations would have been used here, it would have been possible to explicitly compute the SHS response, rather than using a more simplified assumption as was done here. It is also expected that different interaction mechanisms will lead to different intensity or scattering pattern responses. For example, a drastic restructuring of the liposomes (e.g., transformation into bicelles or micelles) will change the second-order nonlinear scattering form factors and thus alter the intensity in a different manner than worked out here. Another example might be a protein or pore that undergoes a drastic change in the charge distribution as this will result in a different (but still quantifiable) change in the effective third-order form factors. Many of such structural and charging effects have been modeled previously.[32−35] Thus, the SHS technique advances the toolbox for quantifying structural biology approaches toward high throughput, smaller samples, and label-free and noninvasive approaches. This will lead to a better understanding of membrane−protein interactions.

In summary, besides QCM, SPR, and floatation assays that are commonly used to determine the protein−membrane binding affinity, we introduced a complementary method, high-throughput second harmonic scattering, that is overcoming many limitations of these techniques. The SHS method enables to mimic the native environment of a membrane protein since the membrane composition and curve could be simulated, bridging the current gap between *in vitro* and *in vivo* experiments. We have shown the ultrasensitive detection of protein liposome interaction in an aqueous solution with a sensitivity in the femtomolar to picomolar range, which translates to a single transmembrane protein being bound to a single liposome. Furthermore, high-throughput SHS can potentially be performed with a small footprint tabletop instrument that uses small sample volumes (<10 μL), instead of 800 μL used in the current study, and small amounts of protein (nM). More importantly, as shown here, it enables the detection of membrane−protein interactions in the low femtomolar regime in a direct, label-free, model-free, and noninvasive manner.

■ ASSOCIATED CONTENT

Supporting Information

The Supporting Information is available free of charge at https://pubs.acs.org/doi/10.1021/acs.jpclett.1c04011.

(S1) Chemicals, (S2) sample preparation, (S3) second-harmonic scattering, and (S4) CryoEM-image acquisition and image processing (PDF)

■ AUTHOR INFORMATION

Corresponding Author

S. Roke − *Laboratory for fundamental BioPhotonics (LBP), Institute of Bio-engineering (IBI), School of Engineering (STI) and Institute of Materials Science (IMX) and Lausanne Centre for Ultrafast Science (LACUS), École Polytechnique Fédérale de Lausanne (EPFL), CH-1015 Lausanne, Switzerland;* orcid.org/0000-0002-6062-7871; Email: sylvie.roke@epfl.ch

Authors

T. Schönfeldová − *Laboratory for fundamental BioPhotonics (LBP), Institute of Bio-engineering (IBI), School of Engineering (STI), École Polytechnique Fédérale de Lausanne (EPFL), CH-1015 Lausanne, Switzerland*

H. I. Okur − *Laboratory for fundamental BioPhotonics (LBP), Institute of Bio-engineering (IBI), School of Engineering (STI), École Polytechnique Fédérale de Lausanne (EPFL), CH-1015 Lausanne, Switzerland; Department of Chemistry and National Nanotechnology Research Center (UNAM), Bilkent University, 06800 Ankara, Turkey;* orcid.org/0000-0002-2492-1168

V. Vezočnik − *Department of Biology, Biotechnical Faculty, University of Ljubljana, Ljubljana 1000, Slovenia*

I. Iacovache − *Institute of Anatomy, University of Bern, 3012 Bern, Switzerland*

C. Cao − *Institute of Bioengineering, School of Life Sciences, École Polytechnique Fédérale de Lausanne (EPFL), 1015 Lausanne, Switzerland;* orcid.org/0000-0003-2592-0690

M. Dal Peraro − *Institute of Bioengineering, School of Life Sciences, École Polytechnique Fédérale de Lausanne (EPFL), 1015 Lausanne, Switzerland;* orcid.org/0000-0002-2973-3975

P. Maček − *Department of Biology, Biotechnical Faculty, University of Ljubljana, Ljubljana 1000, Slovenia;* orcid.org/0000-0001-6470-7759

B. Zuber − *Institute of Anatomy, University of Bern, 3012 Bern, Switzerland;* orcid.org/0000-0001-7725-5579

Complete contact information is available at: https://pubs.acs.org/10.1021/acs.jpclett.1c04011

Funding

S.R. acknowledges the Julia Jacobi Foundation. H.I.O. thanks EU MCSA-IF (Grant No. 899088) for financial support. P.M. and V.V. were supported by the Slovenian Research Agency (grant P1−0207). V.V. acknowledges an EMBO Short-term Fellowship (nr. 7326). B.Z., M.D.P., and C.C. thank the Swiss National Science Foundation (179520 to B.Z., 157217 to M.D.P., and PR00P3_193090 to C.C.). Electron Microscopy was performed with instruments supported by the Microscopy Imaging Center (MIC) of the University of Bern.

Notes

The authors declare no competing financial interest.

■ REFERENCES

(1) Alberts, B.; Johnson, A.; Lewis, J.; Roberts, K.; Raff, M.; Walter, P. *Mol. Biol. Cell*; Garland Science, 2008.

(2) Berg, J. M.; Tymoczko, J. L.; Stryer, L.; Berg, J. M.; Tymoczko, J. L.; Stryer, L. *Biochemistry*, 5th ed.; W H Freeman, 2002.

(3) Dal Peraro, M.; van der Goot, F. G. Pore-Forming Toxins: Ancient, but Never Really out of Fashion. *Nature Reviews Microbiology* **2016**, *14* (2), 77−92.

(4) Hotze, E. M.; Tweten, R. K. Membrane Assembly of the Cholesterol-Dependent Cytolysin Pore Complex. *Biochimica et Biophysica Acta (BBA) - Biomembranes* **2012**, *1818* (4), 1028−1038.
(5) Rossjohn, J.; Feil, S. C.; McKinstry, W. J.; Tweten, R. K.; Parker, M. W. Structure of a Cholesterol-Binding, Thiol-Activated Cytolysin and a Model of Its Membrane Form. *Cell* **1997**, *89* (5), 685−692.
(6) Yilmaz, N.; Kobayashi, T. Assemblies of Pore-Forming Toxins Visualized by Atomic Force Microscopy. *Biochimica et Biophysica Acta (BBA) - Biomembranes* **2016**, *1858* (3), 500−511.
(7) Tilley, S. J.; Orlova, E. V.; Gilbert, R. J. C.; Andrew, P. W.; Saibil, H. R. Structural Basis of Pore Formation by the Bacterial Toxin Pneumolysin. *Cell* **2005**, *121* (2), 247−256.
(8) Reboul, C. F.; Whisstock, J. C.; Dunstone, M. A. A New Model for Pore Formation by Cholesterol-Dependent Cytolysins. *PLoS Comput. Biol.* **2014**, *10* (8), e1003791.
(9) Dang, T. X.; Hotze, E. M.; Rouiller, I.; Tweten, R. K.; Wilson-Kubalek, E. M. Prepore to Pore Transition of a Cholesterol-Dependent Cytolysin Visualized by Electron Microscopy. *J. Struct. Biol.* **2005**, *150* (1), 100−108.
(10) Edvardsson, M.; Svedhem, S.; Wang, G.; Richter, R.; Rodahl, M.; Kasemo, B. QCM-D and Reflectometry Instrument: Applications to Supported Lipid Structures and Their Biomolecular Interactions. *Anal. Chem.* **2009**, *81* (1), 349−361.
(11) Lozeau, L. D.; Rolle, M. W.; Camesano, T. A. A QCM-D Study of the Concentration- and Time-Dependent Interactions of Human LL37 with Model Mammalian Lipid Bilayers. *Colloids Surf., B* **2018**, *167*, 229−238.
(12) Nielsen, S. B.; Otzen, D. E. Impact of the Antimicrobial Peptide Novicidin on Membrane Structure and Integrity. *J. Colloid Interface Sci.* **2010**, *345* (2), 248−256.
(13) Zhao, H.; Lappalainen, P. A Simple Guide to Biochemical Approaches for Analyzing Protein−Lipid Interactions. *MBoC* **2012**, *23* (15), 2823−2830.
(14) Besenič ar, M.; Maček, P.; Lakey, J. H.; Anderluh, G. Surface Plasmon Resonance in Protein−Membrane Interactions. *Chem. Phys. Lipids* **2006**, *141* (1), 169−178.
(15) MacKenzie, C. R.; Hirama, T.; Buckley, J. T. Analysis of Receptor Binding by the Channel-Forming Toxin Aerolysin Using Surface Plasmon Resonance. *J. Biol. Chem.* **1999**, *274* (32), 22604−22609.
(16) Figueira, T. N.; Freire, J. M.; Cunha-Santos, C.; Heras, M.; Gonçalves, J.; Moscona, A.; Porotto, M.; Salomé Veiga, A.; Castanho, M. A. R. B. Quantitative Analysis of Molecular Partition towards Lipid Membranes Using Surface Plasmon Resonance. *Sci. Rep.* **2017**, *7* (1), 45647.
(17) Cooper, M. A.; Try, A. C.; Carroll, J.; Ellar, D. J.; Williams, D. H. Surface Plasmon Resonance Analysis at a Supported Lipid Monolayer. *Biochimica et Biophysica Acta (BBA) - Biomembranes* **1998**, *1373* (1), 101−111.
(18) Haes, A. J.; Van Duyne, R. P. A Nanoscale Optical Biosensor: Sensitivity and Selectivity of an Approach Based on the Localized Surface Plasmon Resonance Spectroscopy of Triangular Silver Nanoparticles. *J. Am. Chem. Soc.* **2002**, *124* (35), 10596−10604.
(19) Seelig, J. Thermodynamics of Lipid−Peptide Interactions. *Biochimica et Biophysica Acta (BBA) - Biomembranes* **2004**, *1666* (1), 40−50.
(20) Sprague, B. L.; McNally, J. G. FRAP Analysis of Binding: Proper and Fitting. *Trends Cell Biol.* **2005**, *15* (2), 84−91.
(21) Sengupta, P.; Jovanovic-Talisman, T.; Skoko, D.; Renz, M.; Veatch, S. L.; Lippincott-Schwartz, J. Probing Protein Heterogeneity in the Plasma Membrane Using PALM and Pair Correlation Analysis. *Nat. Methods* **2011**, *8* (11), 969−975.
(22) Jeong, M. G.; Zhou, K.; Park, S.; An, H.; Kwon, Y.; Chang, Y.; Kim, D.-H.; Ryu, S. H. Analysis of Transient Membrane Protein Interactions by Single-Molecule Diffusional Mobility Shift Assay. *Exp Mol. Med.* **2021**, *53* (2), 291−299.
(23) Tran, R. J.; Sly, K. L.; Conboy, J. C. Revealing the Kinetic Advantage of a Competitive Small-Molecule Immunoassay by Direct Detection. *Anal. Chem.* **2020**, *92* (19), 13163−13171.
(24) Tran, R. J.; Sly, K. L.; Conboy, J. C. Applications of Surface Second Harmonic Generation in Biological Sensing. *Annual Rev. Anal. Chem.* **2017**, *10* (1), 387−414.
(25) Gomopoulos, N.; Lütgebaucks, C.; Sun, Q.; Macias-Romero, C.; Roke, S. Label-Free Second Harmonic and Hyper Rayleigh Scattering with High Efficiency. *Opt. Express* **2013**, *21* (1), 815.
(26) Okur, H. I.; Tarun, O. B.; Roke, S. Chemistry of Lipid Membranes from Models to Living Systems: A Perspective of Hydration, Surface Potential, Curvature, Confinement and Heterogeneity. *J. Am. Chem. Soc.* **2019**, *141* (31), 12168−12181.
(27) Schönfeldová, T.; Piller, P.; Kovacik, F.; Pabst, G.; Okur, H. I.; Roke, S. Lipid Melting Transitions Involve Structural Redistribution of Interfacial Water. *J. Phys. Chem. B* **2021**, *125* (45), 12457−12465.
(28) Scheu, R.; Chen, Y.; de Aguiar, H. B.; Rankin, B. M.; Ben-Amotz, D.; Roke, S. Specific Ion Effects in Amphiphile Hydration and Interface Stabilization. *J. Am. Chem. Soc.* **2014**, *136* (5), 2040−2047.
(29) Gonella, G.; Lütgebaucks, C.; de Beer, A. G. F.; Roke, S. Second Harmonic and Sum-Frequency Generation from Aqueous Interfaces Is Modulated by Interference. *J. Phys. Chem. C* **2016**, *120* (17), 9165−9173.
(30) Lütgebaucks, C.; Gonella, G.; Roke, S. Optical Label-Free and Model-Free Probe of the Surface Potential of Nanoscale and Microscopic Objects in Aqueous Solution. *Phys. Rev. B* **2016**, *94* (19), DOI: 10.1103/PhysRevB.94.195410.
(31) Dedic, J.; Rocha, S.; Okur, H. I.; Wittung-Stafshede, P.; Roke, S. Membrane−Protein−Hydration Interaction of α-Synuclein with Anionic Vesicles Probed via Angle-Resolved Second-Harmonic Scattering. *J. Phys. Chem. B* **2019**, *123* (5), 1044−1049.
(32) de Beer, A. G. F.; Roke, S. Sum Frequency Generation Scattering from the Interface of an Isotropic Particle: Geometrical and Chiral Effects. *Phys. Rev. B* **2007**, *75* (24), DOI: 10.1103/PhysRevB.75.245438.
(33) de Beer, A. G. F.; Roke, S. Obtaining Molecular Orientation from Second Harmonic and Sum Frequency Scattering Experiments in Water: Angular Distribution and Polarization Dependence. *J. Chem. Phys.* **2010**, *132* (23), 234702.
(34) de Beer, A. G. F.; Campen, R. K.; Roke, S. Separating Surface Structure and Surface Charge with Second-Harmonic and Sum-Frequency Scattering. *Phys. Rev. B* **2010**, *82* (23), DOI: 10.1103/PhysRevB.82.235431.
(35) de Beer, A. G. F.; Roke, S.; Dadap, J. I. Theory of Optical Second-Harmonic and Sum-Frequency Scattering from Arbitrarily Shaped Particles. *J. Opt. Soc. Am. B* **2011**, *28*, 1374−1384.

https://doi.org/10.1021/acs.jpclett.1c04011
J. Phys. Chem. Lett. 2022, 13, 3197−3201